

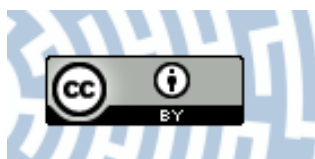


**You have downloaded a document from
RE-BUŚ
repository of the University of Silesia in Katowice**

Title: Luminescence of Agrellite Specimen from the Kipawa River Locality

Author: Maria Czaja, Radosław Lisiecki

Citation style: Czaja Maria, Lisiecki Radosław. (2019). Luminescence of Agrellite Specimen from the Kipawa River Locality. "Minerals" (Vol. 9, iss. 12 (2019), art. no. 752), doi 10.3390/min9120752



Uznanie autorstwa - Licencja ta pozwala na kopiowanie, zmienianie, rozprowadzanie, przedstawianie i wykonywanie utworu jedynie pod warunkiem oznaczenia autorstwa.



UNIwersYTET ŚLĄSKI
W KATOWICACH




Biblioteka
Uniwersytetu Śląskiego



Ministerstwo Nauki
i Szkolnictwa Wyższego

Article

Luminescence of Agrellite Specimen from the Kipawa River Locality

Maria Czaja ^{1,*}  and Radosław Lisiecki ²

¹ Faculty of Natural Sciences, Institute of Earth Sciences, University of Silesia, Będzińska 60, 41-200 Sosnowiec, Poland

² Institute of Low Temperature and Structure Research, Polish Academy of Sciences, W. Trzebiatowski Institute, Okólna 2, 50-422 Wrocław, Poland; r.lisiecki@intibs.pl

* Correspondence: maria.czaja@us.edu.pl

Received: 29 October 2019; Accepted: 30 November 2019; Published: 3 December 2019



Abstract: Using steady-state luminescence measurements, the luminescence spectra of Ce³⁺, Pr³⁺, Nd³⁺, Sm³⁺, Eu³⁺, Dy³⁺, Er³⁺ and Yb³⁺ for the agrellite sample from the Kipawa River region have been measured. The emission spectra of Eu³⁺ and Dy³⁺ next to those of Sm³⁺ and Pr³⁺ have been measured for characteristic excitation conditions. The most efficient luminescence activator in the studied sample was Ce³⁺. This ion was also a sensitizer of Pr³⁺, Sm³⁺, Eu³⁺, and Dy³⁺ luminescence.

Keywords: agrellite; lanthanide ion; energy transfer

1. Introduction

Agrellite is a rather rare mineral and is usually found in pegmatite lenses and pods or in mafic gneisses in a regionally metamorphosed agpatic alkali rock complex. It occurs with eudialyte, britholite, aegirine, as well as miserite, vlasovite, calcite, fluorite, clinohumite, gittinsite, norbergite, zircon, biotite, phlogopite, galena, and quartz. The most known localities of it are the Sheffield Lake complex, Kipawa River, Villedieu Township, Québec (Canada), Dara-i-Pioz massif, Alai Range, Tien Shan Mountains (China), (Tajikistan), the Murun massif, southwest of Olekminsk, Yakutia, (Russia) and Wausau complex, and finally, Marathon Co. in Wisconsin (USA). Among the minerals from the Kipawa River complex, only britholite, fluorite, calcite, miserite, and zircon are predisposed to exhibit fluorescence from lanthanide ions. However, no such reports are known so far. The knowledge of agrellite luminescence comes from websites only [1–3], and from the Gorobets and Rogojine review book [4]. According to these sources, agrellite has a dull pink color or a bright pink color under shortwave ultraviolet (SW UV) or longwave ultraviolet (LW UV, respectively). The following emission centers have been observed [4]: Ce³⁺, Dy³⁺, and Sm³⁺ for samples from the Kipawa River; Fe³⁺, Mn²⁺, Eu²⁺, and presumed Nd³⁺ for samples from the Yakutia; and of Ce³⁺ and Mn²⁺ for specimens from the Dara-i-Pioz. The latest results of spectroscopic investigation of agrellite samples from Dara-i-Pioz (Tajikistan) and Murun massif (Russia) shows luminescence from Ce³⁺ and EPR spectra of Mn²⁺ [5].

An attempt was also made to synthesize sodium calcium silicate with an initial composition such as agrellite [6]. These materials were doped with Mn²⁺ (1%, 2%, and 3%), Ce³⁺ (0.5%), and Tb³⁺ (4%), but as a result of synthesis, multiphase nanoparticles composed of wollastonite 2M CaSiO₃, devitrite Na₂Ca₃Si₆O₁₆, and cristobalite SiO₂ was formed.

The current paper presents the preliminary results of a study of the luminescence properties of agrellite NaCa₂Si₄O₁₀F specimens from the Kipawa Alkaline Complex, Québec, Canada.

Agrellite crystallized in triclinic, space group P(−1), and unit cell parameters are: a = 7.759 (2) Å, b = 18.946 (3) Å, c = 6.986 (1) Å, α = 89.88°, β = 116.65°, γ = 94.34°, Z = 4 [7]. All atoms in the agrellite lattice are present in general positions and the Wyckoff site of all atoms is denoted as 2i. The crystal

structure of agrellite consists of two different NaO_8 distorted cubes polyhedra, two CaO_5F octahedra (hereinafter referred to as Ca1B and Ca2A), and two CaO_6F_2 polyhedra (named as Ca1A and Ca2B) coupled with two different Si_8O_{20} chains [7]. The mean of Ca–O and Ca–F distances are smaller for CaO_5F octahedra and equal for Ca1B and Ca2A, respectively 2.381 Å, 2.192 Å, 2.367 Å, and 2.201 Å than CaO_6F_2 and equal for Ca1A and Ca2B, respectively 2.574, 2.402, 2.615 Å and 2.454 Å (Figure 1a,b).

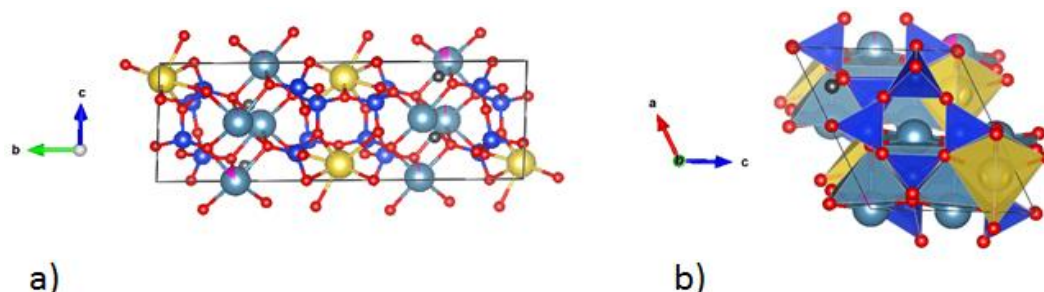


Figure 1. A sketch of agrellite structure: (a) on (100) plane; oxygen atoms—small red balls, silicon atoms—small blue balls, calcium atoms—big blue balls, Ca1A site—big blue and magenta balls, sodium atoms—big yellow balls, and fluorine atoms—small black balls; (b) on (010) plane; small dark blue tetrahedra in Si_8O_{20} chains, big light blue Ca–O, F and yellow NaO_8 polyhedra; small red balls—oxygen atoms.

2. Materials and Methods

The agrellite sample studied here takes the form of fine lath-shaped aggregates measuring from a few to over 100 μm in length. It has a greenish-white color (Figure 2a) which changes to lavender-pink under mid UV (Figure 2b).

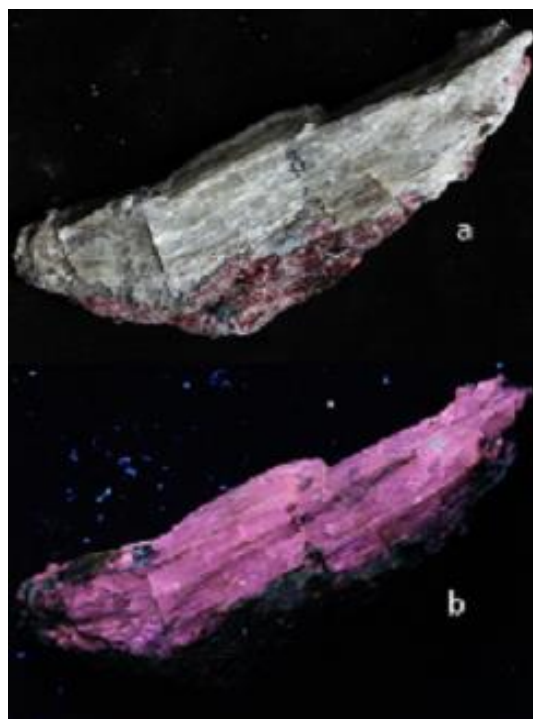


Figure 2. Photos of agrellite sample under white light (a) and LW UV (365 nm) (b).

Rare earth elements (REE) concentrations in the studied agrellite crystal were measured by the ICP-MS method at ACMA Lab (Canada), and the results are listed in Table 1. Steady-state fluorescence measurements for ions shown in the chemical analysis were performed using a Jobin-Yvon (SPEX)

spectrofluorimeter FLUOROLOG 3-12 (Jobin-Yvon, Grenoble, France SPEX at room temperature using a 450 W xenon lamp, a double-grating monochromator, and a Hamamatsu 928 photomultiplier (Hamamatsu Photonics, Shizuoka, Japan). The wavelength range for emission and excitation spectra was from 250 to 900 nm, and the resolution no lower than 1 nm. For such conditions, the emission and excitation spectra of Ce^{3+} , Pr^{3+} , Sm^{3+} , Eu^{3+} , Dy^{3+} , and Er^{3+} in the UV–Vis range were recorded. The emission spectra of Nd^{3+} , Yb^{3+} , and Er^{3+} also in the NIR range were measured utilizing a Dongwoo Optron DM711 monochromator (MaeSan-Ri, Opo-Eup, GwangJu-Si, Gyeonggi-Do, Korea) coupled with a Hamamatsu 928 photomultiplier (Hamamatsu Photonics, Shizuoka, Japan), and an InGaAs detector (Hamamatsu Photonics, Shizuoka, Japan) or PbS detector (Hamamatsu Photonics, Shizuoka, Japan) depending on the spectral region. An InGaAs diode laser (Appolo Instruments, Irvine, USA) emitting infrared radiation at 975 nm and an AlGaAs diode laser (CNI, Changchun, China) emitting at 808 nm were used as continuous wave excitation sources.

Table 1. Concentration of some transition elements in the studied agrellite sample.

Contents (ppm)							
Y	La + Lu	Ce	Pr	Nd	Sm	Eu	Gd
>2000	>2000	>2000	1174	>2000	1034	136	1265
Contents (ppm)							
Tb	Dy	Ho	Er	Tm	Yb	Mn	Fe
221	1419	282	772	93	458	1454	<2000

3. Results

In the studied agrellite specimen, the minimum content of lanthanide ions as a potential luminescence activator can be estimated as 1.0% (Table 1). If the distribution of these ions is uniform, then these ions are present in every 2.5 unit cell. The maximum distance among 4f ions is not less than 17.5 Å and not more than 47.25 Å.

Using steady-state fluorescence measurements, the emission of the following lanthanide ions were measured: Ce^{3+} , Pr^{3+} , Nd^{3+} , Sm^{3+} , Eu^{3+} , Er^{3+} , and Yb^{3+} . Despite the significant Mn content, the emission spectra of Mn^{2+} were not measured. Unlike the [4] data, no emission from Fe^{3+} was obtained.

3.1. Nd^{3+} , Yb^{3+} , and Er^{3+} Luminescence

The emission of Nd^{3+} was measured as a group of three multiples (Figure 3). The most intense was measured at 1046, 1060, 1064, 1078, and 1092 nm and corresponds to the ${}^4F_{3/2} \rightarrow {}^4I_{11/2}$ transition. Another group of lines at 879, 885, 893, 905, and 917 nm is associated with the ${}^4F_{3/2} \rightarrow {}^4I_{9/2}$ transitions and the last with lines at 1313, 1335, and 1340 nm—with the ${}^4F_{3/2} \rightarrow {}^4I_{13/2}$ transitions. The emission spectrum of Yb^{3+} was not very intense (inset of Figure 3) and band 979 nm corresponds to the transition ${}^2F_{5/2} \rightarrow {}^2F_{7/2}$.

It was expected that the measurement of distinct emission lines of Er^{3+} would be possible due to the significant content of this ion and its high luminescence efficiency. However, the emission bands of Er^{3+} corresponding to the ${}^2H_{11/2} \rightarrow {}^4I_{15/2}$, ${}^4S_{3/2} \rightarrow {}^4I_{15/2}$ and ${}^4F_{9/2} \rightarrow {}^4I_{15/2}$ transitions and usually measured at a 500–600 nm range were not clearly visible for steady-state luminescence measurements using a xenon lamp excitation, contrary to time-resolved measurements [8]. It has previously been verified [9] that for steady-time measurements using a xenon lamp, the most convenient excitation for Er^{3+} is $\lambda = 377$ nm. However, for the studied agrellite specimen, only a weak emission band at 543 nm was measured (Figure 4). In the NIR range, the distinct emission band at 1533 nm (1554 nm, 1512 nm, and 1488 nm) was measured as a result of the ${}^4I_{13/2} \rightarrow {}^4I_{15/2}$ transition (Figure 5). Using laser excitation, emission bands of ${}^2H_{11/2} \rightarrow {}^4I_{15/2}$, ${}^4S_{3/2} \rightarrow {}^4I_{15/2}$, and ${}^4F_{9/2} \rightarrow {}^4I_{15/2}$ transitions were also obtained (inset in Figure 5). However, the intensities of these bands at 520 and 550 nm were very weak, not only in comparison with the Er^{3+} emission in the NIR range but also with the Sm^{3+} and Pr^{3+} emission lines,

although the samarium or praseodymium concentration was not much higher than the Er content (Figure 6).

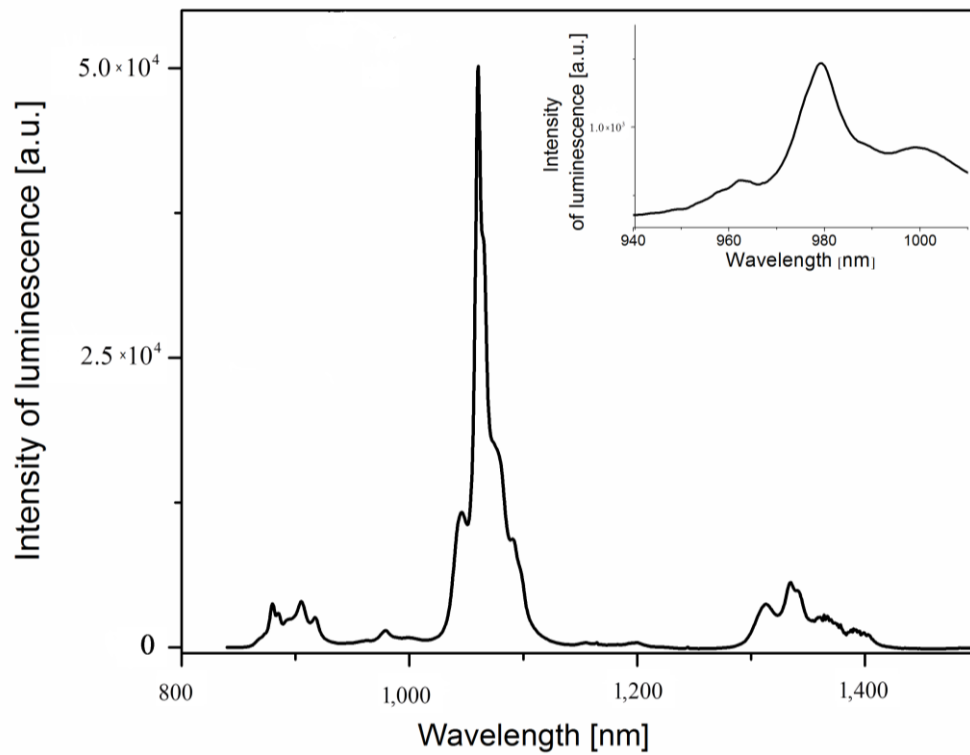


Figure 3. Luminescence spectra of Nd^{3+} and Yb^{3+} in agrellite sample.

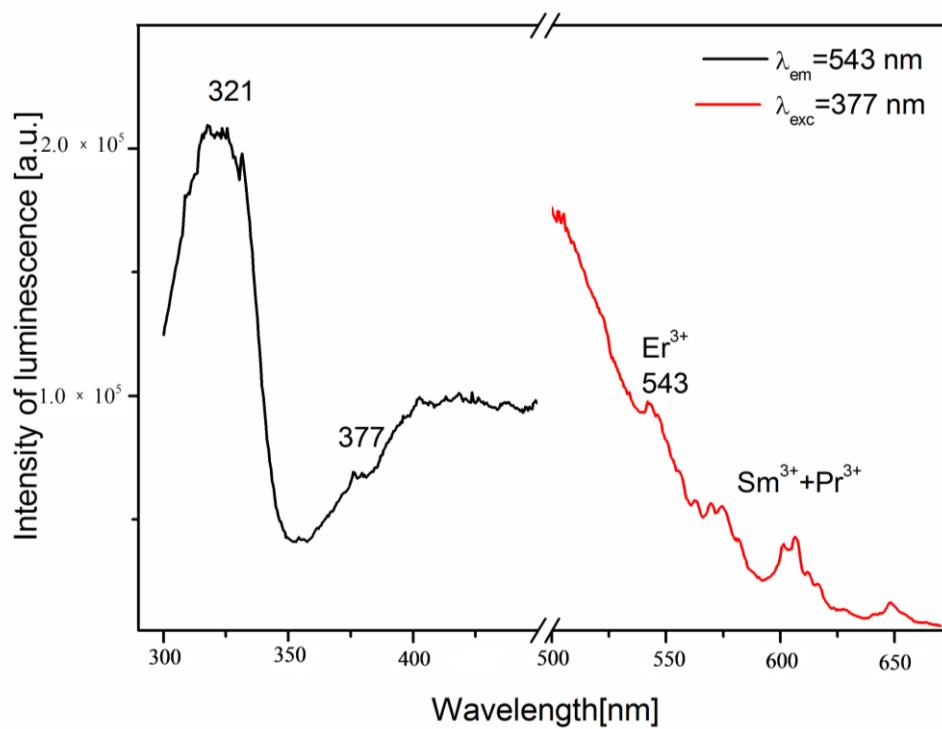


Figure 4. Photoluminescence spectra of Er^{3+} from the agrellite sample.

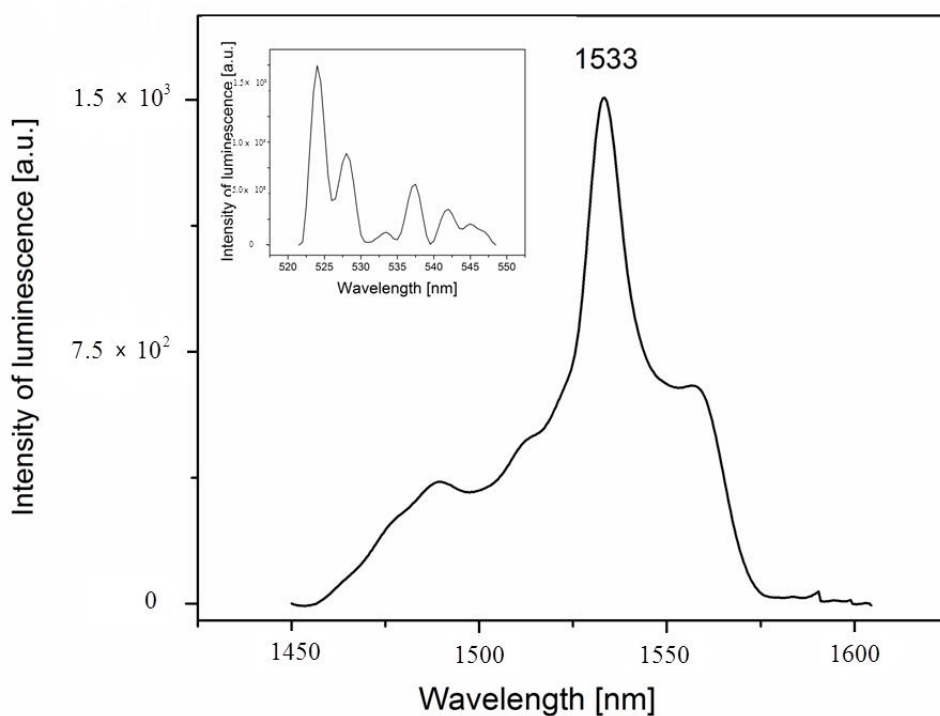


Figure 5. Emission spectra of Er³⁺ from agrellite samples measured under laser excitations.

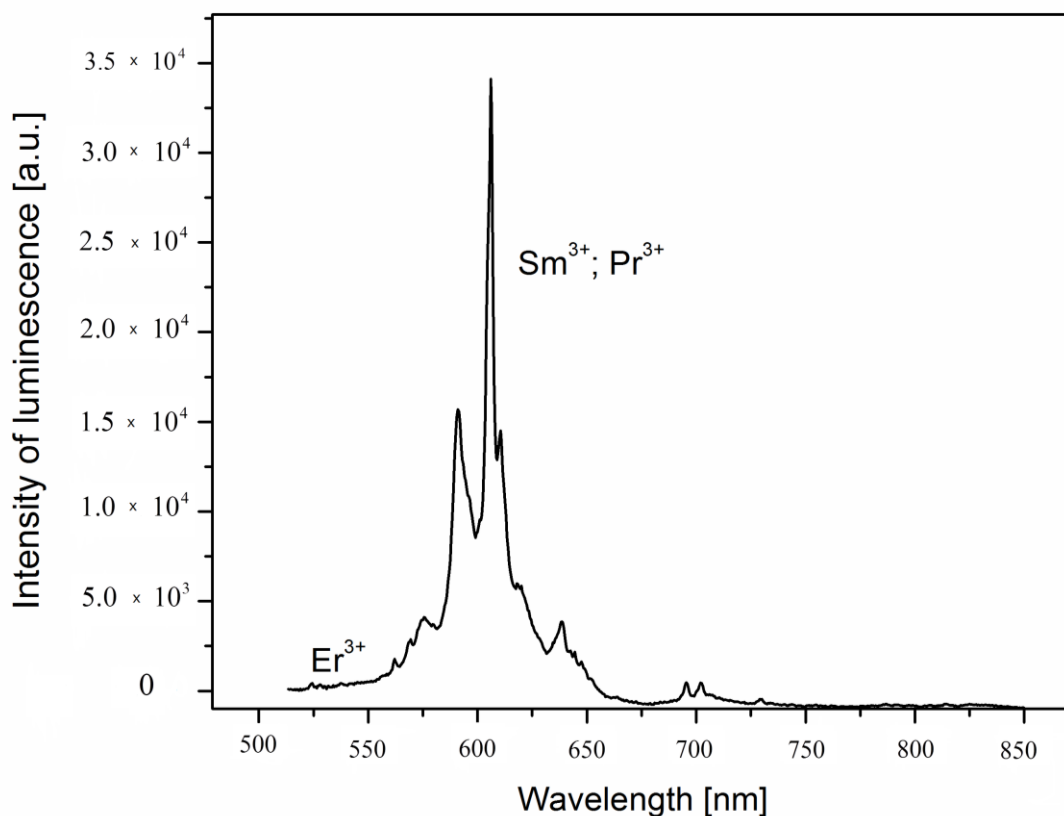


Figure 6. Emission spectra of Sm³⁺, Pr³⁺, and Er³⁺ in Vis range measured under laser excitation.

3.2. Ce³⁺ Fluorescence

The cerium content in the studied agrellite sample was high. Electric-dipole 4f–5d transitions are even and spin allowed with the oscillator strength at half-width and short luminescence decay time.

Cerium Ce^{3+} is often added to synthetic crystals because of its well-known properties as an efficient sensitizer of luminescence. Luminescent materials doped with Ce^{3+} can efficiently absorb excitation energy. A very intensive emission band at 388 nm has been measured (Figure 7). The zero phonon line (ZPL) position was designated in the point of spectral overlap of the excitation and emission curves, i.e., at $\lambda = 337 \text{ nm}$ ($29,673 \text{ cm}^{-1}$). The Stokes shift ΔS , as the energy difference between absorption/excitation and emission maxima of transition between the lowest $5d$ and the $4f$ ground states, is equal to 1567 cm^{-1} . This value is not very high, probably owing to the high coordination number around Ce^{3+} and the long Ca–O distance [10,11]. For the lowest Raman frequency of agrellite 331 cm^{-1} , the Huang-Rhys parameter S is equal to $S = 2.8$, so electron-phonon coupling may be recognized as intermediate.

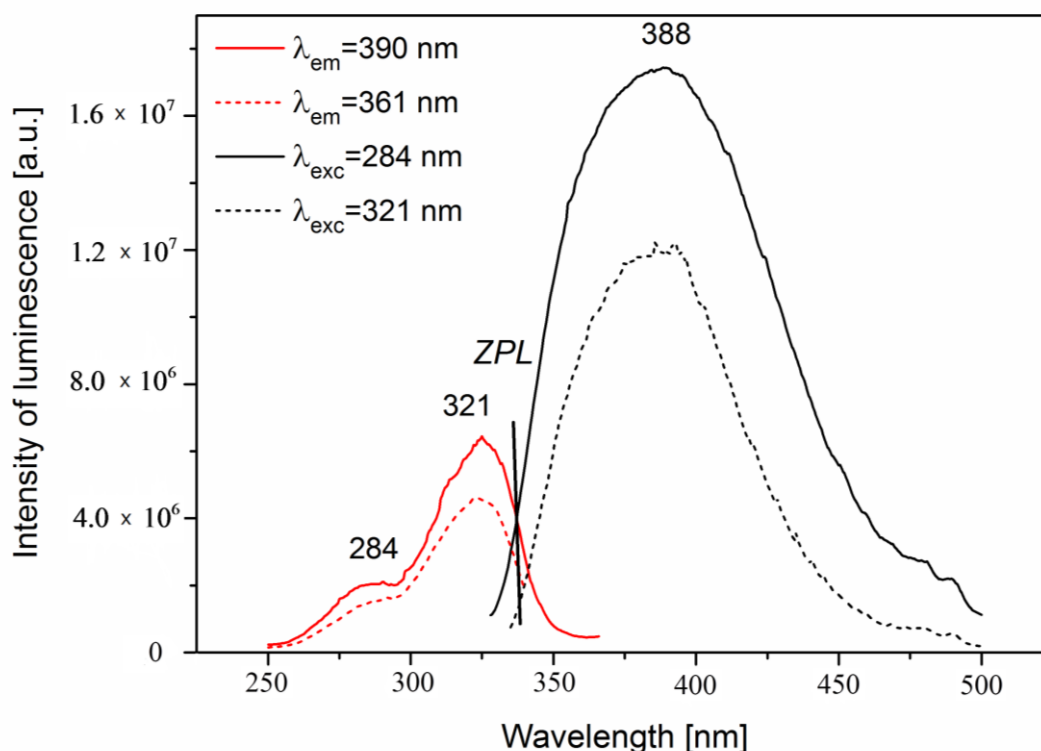


Figure 7. Photoluminescence spectra of Ce^{3+} in agrellite sample.

On the excitation spectra, two bands at 284 nm and 321 nm were recorded, so the crystal-field splitting $10 Dq$ of $5d$ level was estimated as 4059 cm^{-1} . The upper excited level of Ce^{3+} is T_{2g} and the lower is E_g . The $10 Dq$ parameter for Ce^{3+} usually has a value in the $5000\text{--}10,000 \text{ cm}^{-1}$ range. For the studied crystal it was slightly smaller because the Ca–O length in agrellite is larger than in other Ca–minerals, for example fluor-apatite. The emission band of Ce^{3+} is nearly symmetric, although it was fitted to two Gaussian components with maxima at $28,023 \text{ cm}^{-1}$ and $25,819 \text{ cm}^{-1}$ ($R^2 = 0.998$) that can be discerned, (Figure 8), which correspond to the transition terminated on the ${}^2F_{5/2}$ and ${}^2F_{7/2}$ levels.

The intensity of the Ce^{3+} emission band at 388 nm measured for $\lambda_{\text{exc}} = 284 \text{ nm}$ was almost 1.5 times higher than those observed for $\lambda_{\text{exc}} = 321 \text{ nm}$, despite the power of the xenon lamp is lower at $\lambda = 284 \text{ nm}$ than at 321 nm . This may indicate that a significant part of the excitation energy at $\lambda_{\text{exc}} = 321 \text{ nm}$ in the studied mineral transferred to other luminescence centers.

In [5] for the agrellite sample from Dara-i-Pioz, the emission and excitation spectra of Ce^{3+} have been presented. The Ce-content in this sample was 1160–1263 ppm, distinctly less than for the Kipawa River (Table 1). The emission band of Ce^{3+} was measured at 370 nm as a rather symmetrical band, while on the excitation spectrum, the following bands have been measured: 190, 220, 245, 281, and 317 nm. The differences in emission and excitation bands for the sample from Dara-i-Pioz (Tajikistan) and the Kipawa River are certainly due to the change in the Ce–O bonding length in both samples.

It can be concluded that the crystal-field strength for the Kipawa River specimen is less than for the sample from Dara-i-Pioz. The possibility of Ce^{4+} presence and Ce^{4+} charge transfer bands on the absorption spectrum at 400 nm, which may be due to the gray color of agrellite crystals, was also assumed [5].

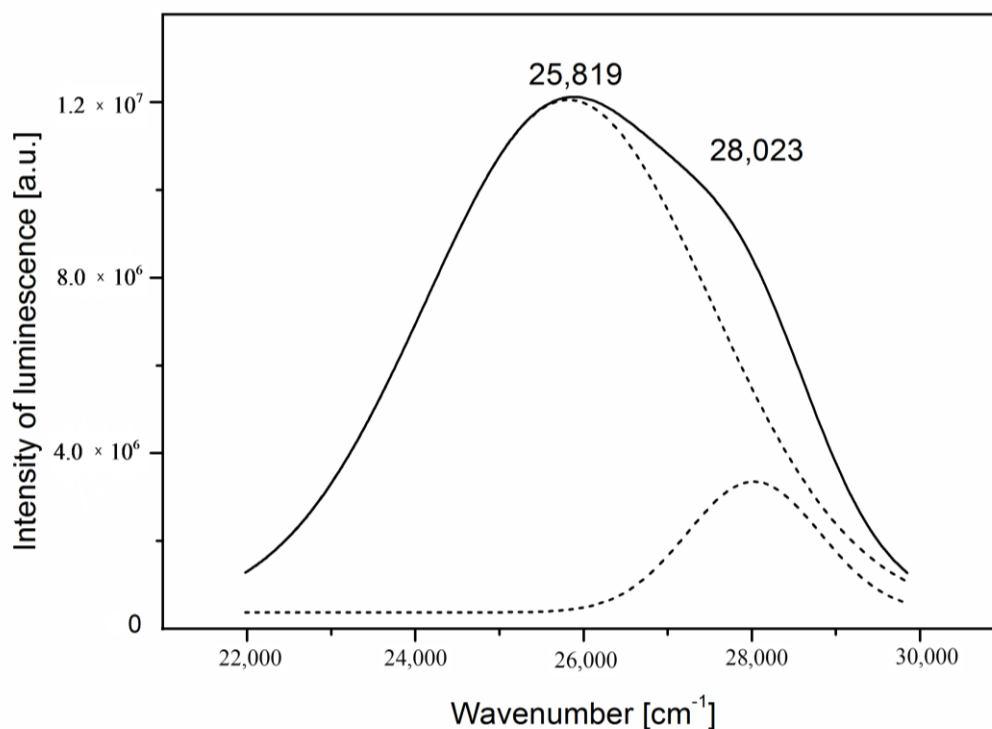


Figure 8. The deconvolution of emission band of $Ce^{3+} E_g(4f5d) \rightarrow 4f (^2F_{5/2}, ^2F_{7/2})$ into two components.

For the studied agrellite sample, the energy transfer between Ce^{3+} and Dy^{3+} , Eu^{3+} , Sm^{3+} , and Pr^{3+} were found. Energy transfer in phosphors with sensitizer-activator ion pairs means that part of the excitation energy of the sensitizer ion transfers to activator ion through a non-radiative process and it subsequently enhances or generates the emission of the activator. The energy transfer among Ce^{3+} and other 4f ions is well known and used to synthesize phosphors with expected properties [12–18].

Gd^{3+} is another activator with intense absorption and emission lines in the UV range. Its excitation line is usually at 275 nm and corresponds to $^8S_{7/2} \rightarrow ^6I_{7/2}$ transition, while emission could occur either from the $^6I_{7/2}$ or the $^6P_{7/2}$ level as a 312 nm band. The Gd^{3+} emission was rarely measured for mineral samples. However, the Gd^{3+} luminescence was found in some scheelite, anhydrite, apatite, and fluorite specimens [19]. Moreover, it was found for CaF_2 [19] that due to energy transfer ($^6I_{7/2} - ^6P_{7/2})(Gd^{3+}) - (^3F_2, ^3H_6 - ^3H_4)(Pr^{3+})$, the emission at 275 nm is weakened, whereas at 312 nm it is enhanced. After using laser induction [4], time-resolved measurements of the Gd^{3+} fluorescence for zircon, anhydrite, and hardystonite have been prepared. The energy transfer among Gd^{3+} and many RE^{3+} have been analyzed [10–27]. For the studied agrellite sample, the energy transfer from Gd^{3+} to RE^{3+} could be excluded. The validity of this thesis is based on the fact that:

- for all substances known from existing literature, the Gd_2O_3 content was about 25 mol% or more.
- the excitation and emission lines of Gd^{3+} did not appear in the agrellite spectra at all, although certain narrow lines should be clearly visible.

3.2.1. Energy Transfer $Ce^{3+} - Dy^{3+}$

The intense emission of Dy^{3+} related to $^4F_{9/2} \rightarrow ^6H_{13/2}$ transition at 575 nm was measured for the most suitable excitation at $\lambda = 438$ nm (solid olive line in Figure 9). However, for $\lambda_{exc} = 321$ nm,

not only was Ce^{3+} emission at 388 nm measured, but so was a Dy^{3+} emission band (solid red lines in Figure 9), and luminescence intensity was stronger than for the previous excitation. Moreover, on the excitation spectrum at $\lambda_{\text{em}} = 575$ nm corresponded to the ${}^4\text{F}_{9/2} \rightarrow {}^6\text{H}_{13/2}$ transition (dash-dot olive line in Figure 9), while the excitation band at 321 nm prevails on the Dy^{3+} band. It appears that the Ce^{3+} excitation band overlapped on the Dy^{3+} $4f^9-4f^85d$ broadband or that it is transferred to the ${}^4\text{K}_{15/2, 17/2}$ excited Dy^{3+} level.

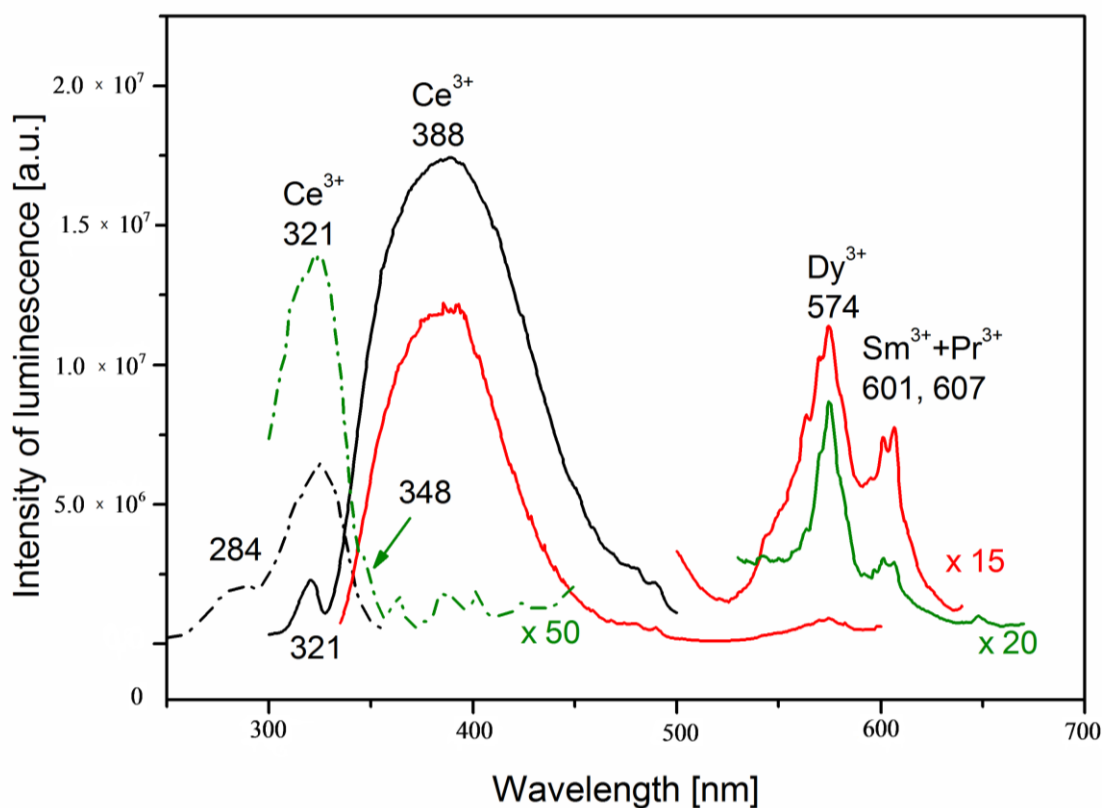


Figure 9. The photoluminescence spectra of Dy^{3+} , Sm^{3+} , and Pr^{3+} and Ce^{3+} . Solid lines—emission spectra: black— $\lambda_{\text{exc}} = 284$ nm, red— $\lambda_{\text{exc}} = 321$ nm, olive line— $\lambda_{\text{exc}} = 348$ nm. Dash-dot lines—excitation spectra: dark olive line— $\lambda_{\text{em}} = 575$ nm, black line— $\lambda_{\text{em}} = 388$ nm.

3.2.2. Energy Transfer Ce^{3+} - Sm^{3+} , Pr^{3+} , and Eu^{3+}

The efficient emission of Sm^{3+} and Pr^{3+} was also found for agrellite crystal. In the spectral range of 550–700 nm, the emission lines of these two ions are located close to each other and are: at 562 nm and 569 nm as ${}^4\text{G}_{5/2} \rightarrow {}^6\text{H}_{5/2}$ transition of Sm^{3+} ; at 601 nm and 607 nm of both Sm^{3+} ${}^4\text{G}_{5/2} \rightarrow {}^6\text{H}_{7/2}$ and Pr^{3+} ${}^1\text{D}_2 \rightarrow {}^3\text{H}_4 + {}^3\text{P}_0 \rightarrow {}^3\text{H}_6$ transitions; and at 648 nm mainly for Pr^{3+} transition ${}^3\text{P}_0 \rightarrow {}^3\text{F}_2$. As it was found earlier [9], the most convenient excitation for Sm^{3+} is the 399–402 nm line, while for Pr^{3+} it is 480 nm (Figure 10).

For $\lambda_{\text{exc}} = 402$ nm excitation, beside of Sm^{3+} and Pr^{3+} emission lines, the Eu^{3+} emission at 613 nm attributed to transition ${}^5\text{D}_0 \rightarrow {}^7\text{F}_2$ have been measured as well (Figure 11).

No emission of Eu^{2+} was found. The emission of Eu^{3+} as a characteristic line at 613 nm was obtained for the most convenient excitation $\lambda_{\text{exc}} = 393$ nm (Figure 12). However, this excitation also caused Sm^{3+} and Pr^{3+} emission.

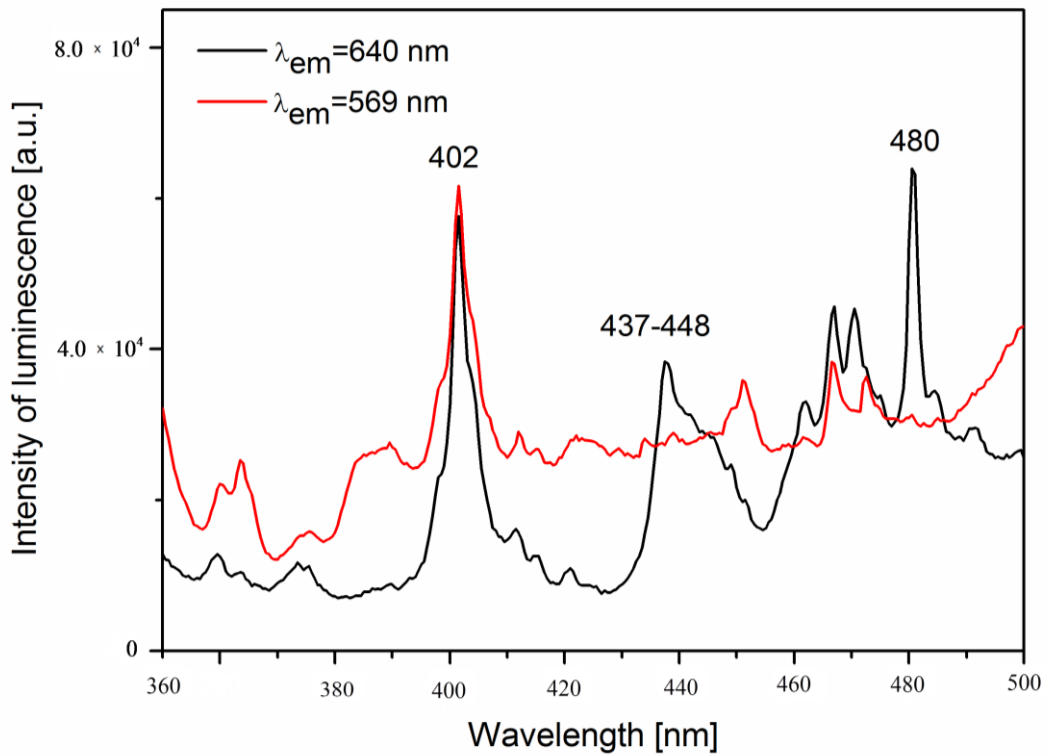


Figure 10. Excitation spectra characteristic for Pr³⁺ (black line) and Sm³⁺ (red line).

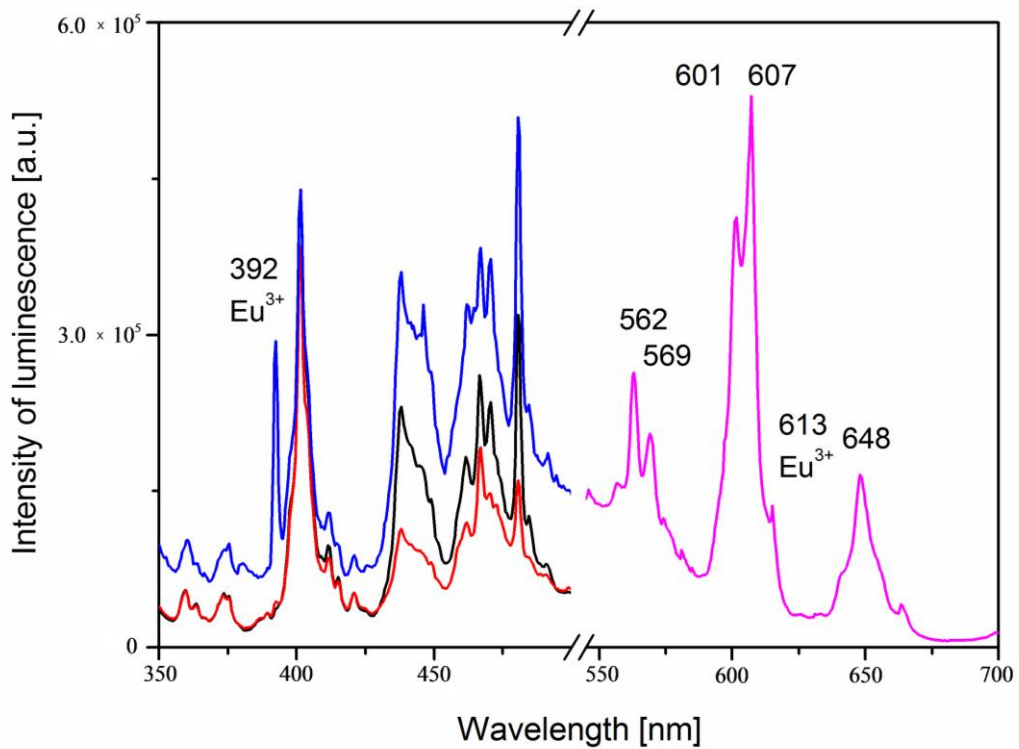


Figure 11. The photoluminescence spectra of Pr³⁺, Sm³⁺, and Eu³⁺ in agrellite. Emission spectrum measured at λ_{exc} = 402 nm excitation—magenta line, excitation spectrum at λ_{em} = 613 nm—blue line, excitation spectrum at λ_{em} = 601 nm—red line, and excitation spectrum at λ_{em} = 648 nm—black line.

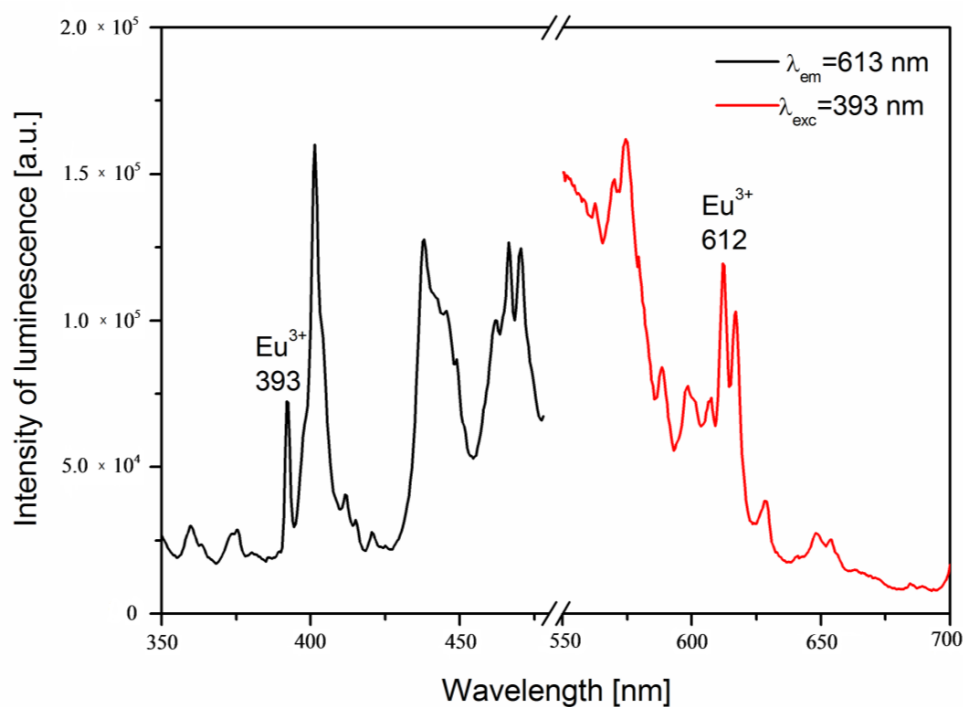


Figure 12. Excitation and emission spectra of Eu^{3+} in agrellite.

Under excitation $\lambda_{\text{exc}} = 321$ nm, not only the emission of Dy^{3+} (574 nm) but also of Sm^{3+} and Pr^{3+} (562 nm, 569 nm, 601 nm, 607 nm), was measured (Figure 9). On the excitation spectra monitored at 562 nm, not only the most convenient bands for Sm^{3+} (and Pr^{3+}) were measured but an intense band of Ce^{3+} was recorded too. In the excitation spectra of Sm^{3+} , Pr^{3+} , and Eu^{3+} , the Ce^{3+} band at 321–323 nm always appeared and it was intense. (Figure 13). This same effect has been measured when luminescence was excited into the Ce^{3+} emission band, i.e., 388 nm (Figure 14).

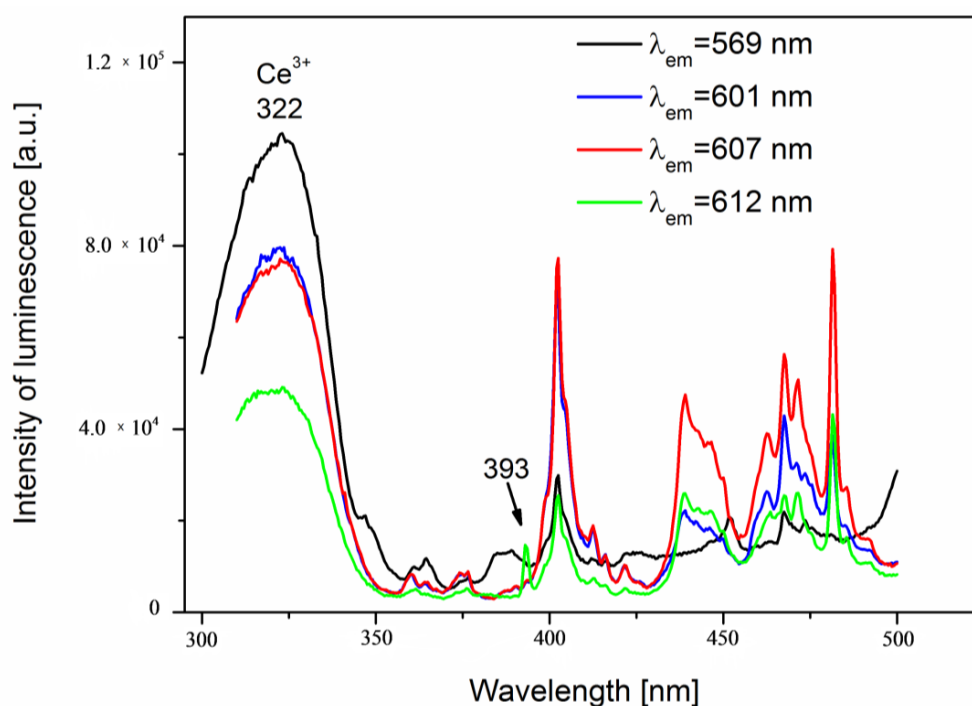


Figure 13. The excitation spectra of Pr^{3+} and Sm^{3+} emission in agrellite.

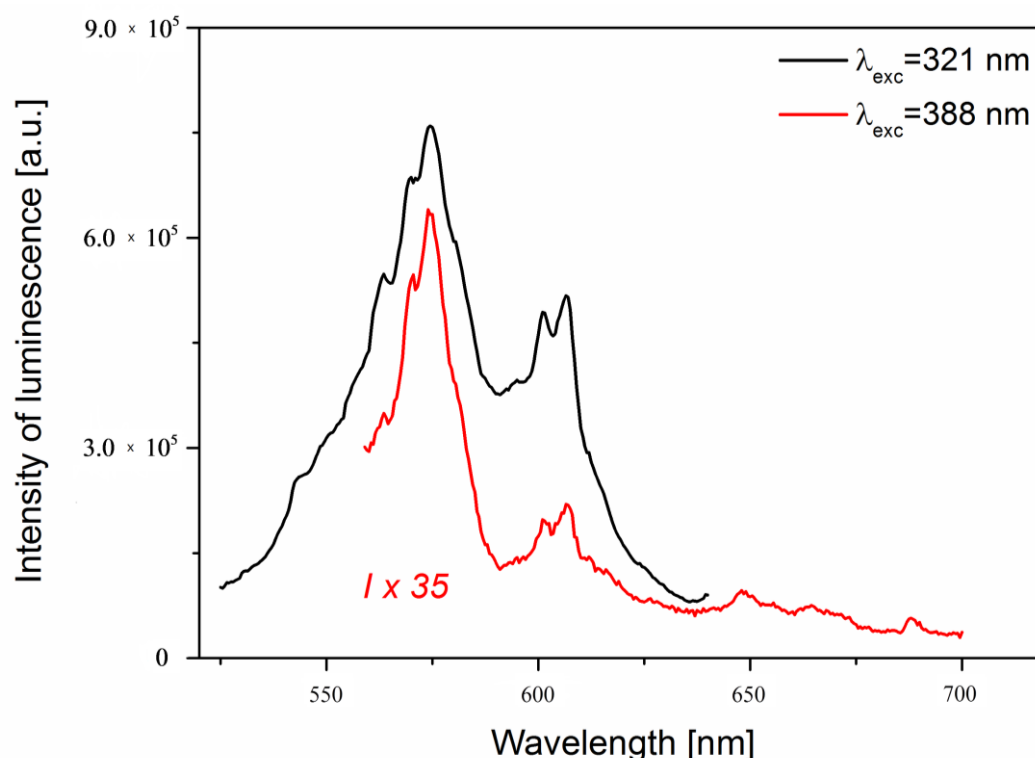


Figure 14. The emission spectra of Pr^{3+} and Sm^{3+} under Ce^{3+} excitations.

The presence of the Ce^{3+} excitation band in the PLE spectrum of Dy^{3+} , Sm^{3+} , Pr^{3+} , and Eu^{3+} indicated the occurrence of $\text{Ce}^{3+} \rightarrow (\text{Dy}^{3+}, \text{Sm}^{3+}, \text{Pr}^{3+}, \text{and } \text{Eu}^{3+})$ energy transfer process. Upon UV irradiation, electrons from the ${}^2\text{F}_{5/2}$ ground state of Ce^{3+} are excited into the 5d excited state. Some of these electrons return to the ground states (${}^2\text{F}_{7/2}$ and ${}^2\text{F}_{5/2}$) of Ce^{3+} ions, resulting in the violet-blue emissions of Ce^{3+} due to the 5d \rightarrow 4f transition. At the same time, owing to the nonradiative resonant energy-transfer, a portion of excited electrons can be transferred into the ${}^4\text{K}_{15/2, 17/2}$ excited levels of Dy^{3+} and then relax, mainly as ${}^4\text{F}_{9/2} \rightarrow {}^6\text{H}_{13/2}$ transition. Similarly, another portion of excited electrons can be transferred into excited levels of ${}^4\text{K}_{11/2}$ or ${}^3\text{P}_2$ of Sm^{3+} or Pr^{3+} and subsequently, the electrons can relax to their ground levels.

4. Conclusions

In the studied agrellite crystal, the lanthanide ions form a complex arrangement of luminescence centers. The f-f emission of many ions has been distinctly excited by the excitation band of Ce^{3+} . Generally, the mechanism of energy transfer from donor to acceptor ions can be attributed to an exchange interaction or electric multipolar interaction. The average distance R_c between the Ce^{3+} donors and Sm^{3+} or Pr^{3+} acceptors was estimated as a value according to the below equation where C is the total concentration of $4f^n$ ions in the studied sample, N is the coordination number, and V is the cell volume:

$$R_c = 2 \sqrt[3]{\frac{3 \cdot V}{4\pi \cdot C \cdot N}}$$

when this value was determined to be 19.38 Å and it is greater than 5 Å, the energy transfer process would take place via electric multipolar interaction. The direct confirmation of this conclusion could be obtained by measuring the decay lifetimes of Ce^{3+} , Dy^{3+} , Sm^{3+} , and Pr^{3+} emissions, as well as the changes in luminescence intensities of these ions for samples containing their variable content. It is necessary to carry out measurements for other specimens of agrellite, differing in the content of these ions.

Contrary to the information on the website [3], the luminescence of Mn^{2+} has not been observed, although it was stated at 580 nm; similarly, no emission band of Eu^{2+} which was notified at 410 nm was observed. Additionally, the emission lines of Dy^{3+} at 478 nm or of Er^{3+} at 522 nm were not clear. It was observed that the measured emission spectra in the 400–560 nm range show intensive scattering of incident radiation not related to the effect of light reflection from the crystal surface. It can be assumed that it is due to the presence of numerous defects on $[\text{Si}_4\text{O}_{10}]^{4-}$ and will be confirmed after femtosecond excitation measurements.

Some differences have been observed between the emission spectra of agrellite specimens for various localities presented in [4] or [5] and our results. The main reason for these differences is certainly the difference in REE content, although the data contained in [1,2] are incomplete. The agrellite specimen from the Kipawa River studied in the current research contains more Ce and a comparable amount of Mn and Fe as a sample from Dara-i-Pioz, and it is more than the sample from Yakutia [5]. However, contrary to [1] but similar to [5], we did not measure the emission of Mn^{2+} as was stated for the specimen from Dara-i-Pioz, and also the emission of $\text{Fe}^{3+}_{\text{tetra}}$ and Eu^{2+} as was shown for the specimen from Yakutia. Compared to previous luminescence results for specimens from the Kipawa River [4], the emissions from Er^{3+} , Pr^{3+} , and Eu^{3+} were also measured in the current research.

The most important result of the present research is the demonstration of the phenomenon of effective energy transfer between Ce^{3+} as a donor and Pr^{3+} , Sm^{3+} , and Dy^{3+} as the acceptors. For this reason, a synthetic material based on agrellite, subsidized with the right amount of these ions, can be an efficient white light emitter.

Author Contributions: Conceptualization, M.C.; Investigation/Measurements, M.C. and R.L.; Resources, M.C.; Original Draft Preparation, M.C.; Writing—Review and Editing and Visualization, M.C. and R.L.

Funding: This research project was supported by the Polish National Science Centre (Grant DEC-2011/03/B/ST10/06320) and by statutory funding from the Faculty of Natural Sciences, Institute of Earth Sciences, University of Silesia.

Conflicts of Interest: The authors declare no conflict of interest.

References

1. Common Fluorescent Minerals. Available online: <https://www.uvminerals.org/minerals/common-fluorescent-minerals> (accessed on 25 October 2019).
2. Agrellite. Available online: http://classicgems.net/gem_agrellite.htm (accessed on 25 October 2019).
3. Online Database of Luminescent minerals. Available online: <http://www.fluomin.org/uk/accueil.php> (accessed on 25 October 2019).
4. Gorobets, B.S.; Rogojine, A.A. *Luminescent Spectra of Minerals*; RPC VIMS: Moscow, Russia, 2002; 300p.
5. Kaneva, E.; Shendrik, R.; Mesto, E.; Bogdanov, A.; Vladykin, N. Spectroscopy and chemical properties of $\text{NaCa}_2[\text{Si}_4\text{O}_{10}]\text{F}$ natural agrellite with tabular structure. *Chem. Phys. Lett.* **2020**, *738*, 136868. [CrossRef]
6. Mickens, M.A.; Assefa, Z. Tunable luminescence and white light emission of novel multiphase sodium calcium silicate nanophosphors doped with Ce^{3+} , Tb^{3+} , and Mn^{2+} ions. *J. Lumin.* **2014**, *145*, 498–506. [CrossRef]
7. Ghose, S.; Wan, C. Agrellite, $\text{Na}(\text{Ca},\text{RE})_2\text{Si}_4\text{O}_{10}\text{F}$: A layer structure with silicate tubes. *Am. Mineral.* **1979**, *64*, 563–572.
8. Gaft, M.; Reisfeld, R.; Panczer, G. *Luminescence Spectroscopy of Minerals and Materials*; Springer: Berlin/Heidelberg, Germany, 2005; 606p.
9. Czaja, M.B.; Bodył-Gajowska, S.; Mazurak, Z. Steady-state luminescence measurement for qualitative identification of rare earth ions in minerals. *J. Miner. Petrol. Sci.* **2013**, *108*, 47–54. [CrossRef]
10. Wang, S.; Song, Z.; Kong, Y.; Liu, Q. Relationship of Stokes shift with composition and structure in $\text{Ce}^{3+}/\text{Eu}^{2+}$ -doped inorganic compounds. *J. Lumin.* **2019**, *212*, 250–263. [CrossRef]
11. Dorenbos, P.; Andriessen, J.; Marsman, M.; van Eik, C.W.E. On the Stokes shift of the Ce^{3+} 5d4f luminescence in inorganic crystals. *Radiat. Eff. Defects Solids* **2001**, *154*, 237–241. [CrossRef]
12. Zhang, J.; Wang, L.; Jin, Y.; Zhang, X.; Hao, Z.; Wang, X. Energy transfer in $\text{Y}_3\text{Al}_5\text{O}_{12}$: Ce^{3+} , Pr^{3+} and CaMoO_4 : Sm^{3+} , Eu^{3+} phosphors. *J. Lumin.* **2011**, *131*, 429–432. [CrossRef]

13. Grzyb, T.; Runowski, M.; Lis, S. Facile synthesis, structural and spectroscopic properties of GdF_3 : Ce^{3+} , Ln^{3+} ($\text{Ln}^{3+} = \text{Sm}^{3+}, \text{Eu}^{3+}, \text{Tb}^{3+}, \text{Dy}^{3+}$) nanocrystals with bright multicolor luminescence. *J. Lumin.* **2014**, *154*, 479–486. [[CrossRef](#)]
14. Caldiño, U.; Lira, A.; Meza-Rocha, A.N.; Pasquini, E.; Pelli, S.; Speghini, H.; Bettinelli, M.; Righini, G.C. White light generation in Dy^{3+} - and $\text{Ce}^{3+}/\text{Dy}^{3+}$ -doped zinc–sodium–aluminosilicate glasses. *J. Lumin.* **2015**, *167*, 327–332. [[CrossRef](#)]
15. Zeng, H.; You, F.; Peng, H.; Huang, S. Energy transfer from Ce^{3+} to Tb^{3+} , Dy^{3+} and Eu^{3+} in $\text{Na}_3\text{Y}(\text{BO}_3)_2$. *J. Rare Earths* **2015**, *33*, 1051–1055. [[CrossRef](#)]
16. Nair, G.B.; Dhoble, S.J. White light emission through efficient energy transfer from Ce^{3+} to Dy^{3+} ions in $\text{Ca}_3\text{Mg}_3(\text{PO}_4)_4$ matrix aided by Li^+ charge compensator. *J. Lumin.* **2017**, *192*, 1157–1166. [[CrossRef](#)]
17. Li, B.; Huang, X.; Lin, J. Single-phased white-emitting $\text{Ca}_3\text{Y}(\text{GaO})_3(\text{BO}_3)_4$: Ce^{3+} , Tb^{3+} , Sm^{3+} phosphors with high-efficiency: Photoluminescence, energy transfer and application in near-UV-pumped white LEDs. *J. Lumin.* **2018**, *204*, 410–418. [[CrossRef](#)]
18. Dev, K.; Selot, A.; Nair, G.B.; Barai, V.L.; Haque, F.Z.; Aynyas, M.; Dhoble, S.J. Energy transfer from Ce^{3+} to Dy^{3+} ions for white light emission in $\text{Sr}_2\text{MgAl}_{22}\text{O}_{36}:\text{Ce}^{3+}, \text{Dy}^{3+}$ phosphor. *J. Lumin.* **2019**, *206*, 380–385. [[CrossRef](#)]
19. Tarashchan, A.N. *Luminescence of Minerals*; Naukova Dumka: Kiev, Ukraine, 1978.
20. Lisiecki, R.; Głowacki, M.; Berkowski, M.; Ryba-Romanowski, W. Contribution of energy transfer process to excitation and relaxation of Yb^{3+} ions in $\text{Gd}_3(\text{Al,Ga})_5\text{O}_{12}:\text{Re}^{3+}, \text{Yb}^{3+}$ ($\text{RE}^{3+} = \text{Tm}^{3+}, \text{Er}^{3+}, \text{Ho}^{3+}, \text{Pr}^{3+}$). *J. Lumin.* **2019**, *211*, 54–61. [[CrossRef](#)]
21. Kaur, P.; Singh, D.; Sing, T. Sm^{3+} and Gd^{3+} Co-doped lead phosphate glasses for γ -rays shielding and sensing. *J. Lumin.* **2019**, *209*, 74–88. [[CrossRef](#)]
22. Khan, I.; Rooh, G.; Rajaramakrishna, R.; Sirsittipokakun, N.; Kim, H.J.; Wondeeying, C.; Kaewkhao, J. Development of Eu^{3+} doped $\text{Li}_2\text{O}-\text{BaO}-\text{GdF}_3-\text{SiO}_2$ oxyfluoride glass for efficient energy transfer from Gd^{3+} to Eu^{3+} in red emission solid state device application. *J. Lumin.* **2018**, *203*, 515–524. [[CrossRef](#)]
23. Fan, B.; Qi, S.; Zhao, W.; Li, S.; An, S. Photoluminescence properties and energy transfer of red phosphors $\text{Y}_2\text{P}_4\text{O}_{13}:\text{Gd}^{3+}, \text{Eu}^{3+}$. *J. Lumin.* **2018**, *196*, 520–524. [[CrossRef](#)]
24. Gupta, P.; Bedyal, A.K.; Kumar, V.; Khajuria, Y.; Sharma, V.; Ntwaeaborwa, O.M.; Swart, H.C. Energy transfer mechanism from Gd^{3+} to Sm^{3+} in $\text{K}_3\text{Gd}(\text{PO}_4)_2:\text{Sm}^{3+}$ phosphor. *Mater. Res. Express* **2015**, *2*, 076202. [[CrossRef](#)]
25. Wantana, N.; Kaewjaeng, S.; Kothan, S.; Kim, H.J.; Kaewkhao, J. Energy transfer from Gd^{3+} to Sm^{3+} and luminescence characteristics of $\text{CaO}-\text{Gd}_2\text{O}_3-\text{SiO}_2-\text{B}_2\text{O}_3$ scintillating glasses. *J. Lumin.* **2017**, *181*, 382–386. [[CrossRef](#)]
26. Liu, C.; Liu, J.; Lu, S.; Chen, B.; Zhang, J. Energy migration and transfer of $\text{Tm}^{3+}-\text{Gd}^{3+}-\text{Dy}^{3+}$ system in NaGdF_4 under VUV and UV excitations. *J. Lumin.* **2007**, *122*, 970–972. [[CrossRef](#)]
27. Reisfeld, R.; Greenberg, E.; Biron, E. Energy transfer between Gd^{3+} and Sm^{3+} . The effect of Gd^{3+} on quenching of Sm^{3+} and intensity parameters of Sm^{3+} in borate glasses. *J. Solid State Chem.* **1974**, *9*, 224–233. [[CrossRef](#)]

